ACS APPLIED MATERIALS & INTERFACES

www.acsami.org

Research Article

Phase-Transitional Ionogel-Based Supercapacitors for a Selective Operation

Jinwoo Park and Jeong-Yun Sun*

Cite This: *ACS Appl. Mater. Interfaces* 2022, 14, 23375−23382

Read Online

ACCESS | Metrics & More | Article Recommendations | Supporting Information

ABSTRACT: As the demand for energy storage devices increases, the importance of electrolytes for supercapacitors (SCs) is further emphasized. However, since ions in electrolytes are always in an active state, it is difficult to store energy for a long time due to ion diffusion. Here, we have synthesized a phase-transitional ionogel and fabricated an SC based on the ionogel. The 1-ethyl-3-methylimidazolium nitrate ($[EMIM]^+[NO_3]^-$) ionogel changes its phase from crystal to amorphous when the temperature was elevated above its phase transition temperature (~44 °C). When the temperature is elevated from 25 to 45 °C, the resistivity of the gel is decreased from 2318.4 kΩ·cm to 43.2 Ω·cm. At the same time, the capacitance is boosted from 0.02 to 37.35 F g^{-1}, and this change was repeatable. Furthermore, the SC exhibits an energy density of 7.77 Wh kg^{-1} with a power density of 4000 W kg^{-1} at 45 °C and shows a stable capacitance retention of 87.5% after 3000 cycles of test. The phase transition can switch the SCs from "operating mode" to "storage mode" when the temperature drops. A degree of self-discharge is greatly suppressed in the storage mode, storing 89.51% of charges after 24 h in self-discharge tests.

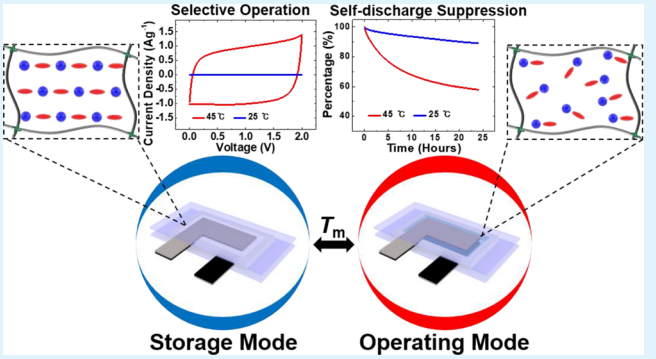

KEYWORDS: *supercapacitor, ionogel electrolyte, phase transition, high density energy storage, suppressed self-discharge*

INTRODUCTION

With the rapid development of society and the emergence of new industries, the ever-increasing demand of energy has increased a need for more efficient energy storage systems. Electric double layer capacitors, also known as supercapacitors (SCs), are representative electrochemical energy storage systems that meet these needs. SCs are electrostatically charged through charge separation at both the high-surface area porous electrode/electrolyte interfaces.[1] They can be charged/discharged in a short period of time and are capable of withstanding a few thousand cycles.[2] These properties allow SCs to be used in vehicles, portable electronics, and military sectors[3] wherever there is a need to release a large amount of stored energy in a short time. However, SCs have a very high self-discharge, making them difficult to sustain a state of charge for a long time. Therefore, various factors have been studied to reduce the self-discharge.[4] One of the main factors of the self-discharge is movement of ions in the electrolyte. In order to control ion mobility, electrodes with stronger interactions with ions are developed,[5] or separators[6] and additives[7,8] were combined with electrolytes to suppress the movement of the ions. However, the self-discharge of SCs basically occurs because ions are always activated in the electrolyte. Therefore, it is expected that the self-discharge of the SCs can be effectively lowered if the movement of ions is deactivated when the SCs are not used.

A phase transition is a method that dramatically changes the flow of ions with temperature. Since ions are crystallized or decrystallized depending on the phase, the movement of ions can be easily controlled according to the temperature. One of the ionic materials that can undergo a phase transition at ambient temperature is an ionic liquid. Ionic liquids (ILs) refer to compounds composed of ions with melting points below 100 °C,[9] and some ILs change phases at their melting point. By using a phase-transitional IL, it is possible to dramatically change the mobility of ions.[10] Additionally, ILs are characterized by very low vapor pressure, high thermal stability, high ionic conductivity, and electrochemical stability.[11] These features make ILs suitable to be used as an electrolyte in an SC, and various studies have been conducted based on them.[12,13] Based on these characteristics, by applying phase-transitional ILs to SCs as electrolytes, it is expected that the activation degree of SCs can be controlled according to the temperature. That is, when the temperature is elevated above the melting point, SCs become active and are operated as an

Received: February 4, 2022
Accepted: May 3, 2022
Published: May 12, 2022

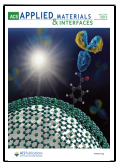

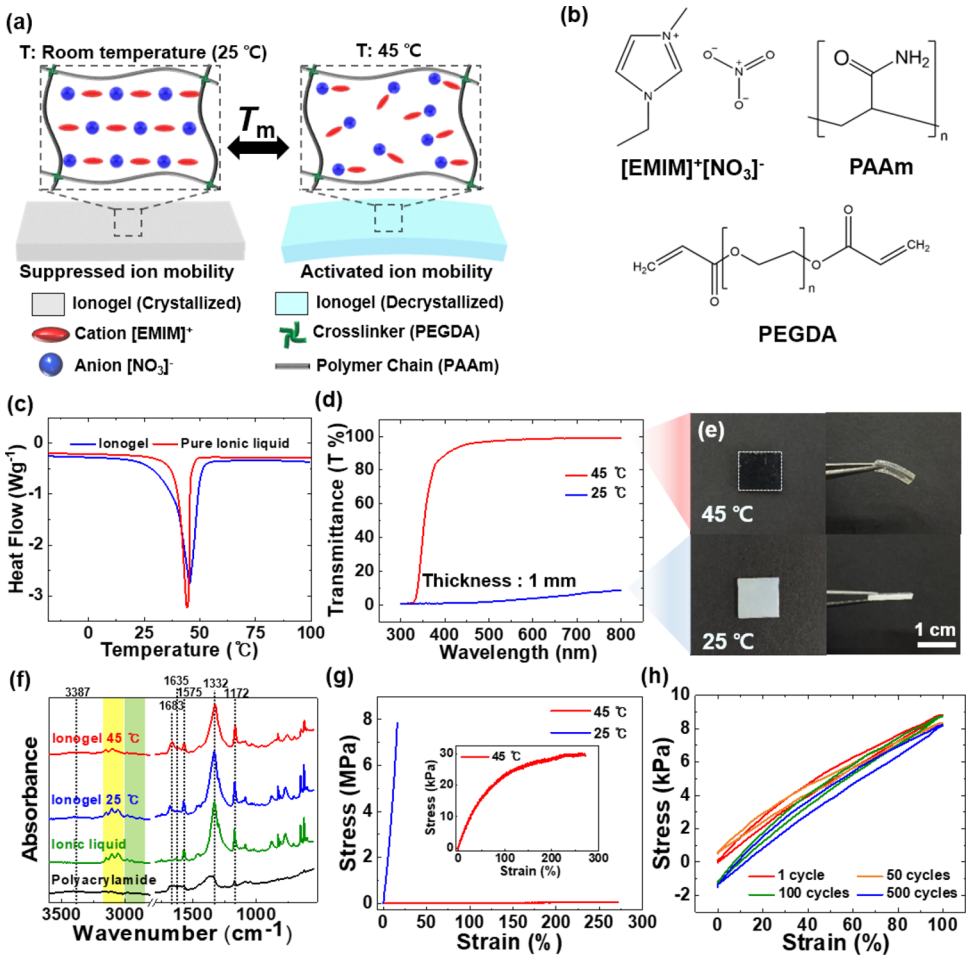

Figure 1. Phase transition of the $[EMIM]^+[NO_3]^-$/PAAm ionogel. (a) Schematic illustration of phase transition of the $[EMIM]^+[NO_3]^-$ ionic liquid in a PAAm network. The ion movement is suppressed or activated based on temperature-triggered phase transformation of ionic liquid (IL) in the ionogel. (b) Structural formulas of phase-transitional IL ($[EMIM]^+[NO_3]^-$), and monomer (PAAm) and crosslinker (PEGDA) miscible with the IL. (c) Differential scanning calorimetry (DSC) curves of the pure $[EMIM]^+[NO_3]^-$ IL and $[EMIM]^+[NO_3]^-$/PAAm ionogel. (d) UV−vis spectra of the ionogel at 25 and 45 °C. Transmittance of the ionogel was shifted from 1 to 99% under 25 °C of ambient temperature. (e) Photographs of ionogels under 45 and 25 °C of ambient temperature. The ionogel containing excited IL exhibited soft and transparent properties, while the ionogel containing crystallized IL exhibited rigid and opaque properties. (f) Fourier-transform infrared spectroscopy (FT-IR) spectrum of freeze-dried polyacrylamide, pure ionic liquid at 25 °C, and the ionogel at 25 and 45 °C. (g) Stress−strain curves of the ionogel at 25 and 45 °C. The inset shows the stress−strain curve of the ionogel at 45 °C. (h) Tensile cyclic stress−strain curves of the ionogel at 45 °C up to a strain of 100%.

energy source. On the other hand, SCs reach an inactive state by lowering the temperature to suppress the movement of ions. In the inactive state, SCs are able to store the energy for a long time.

Here, we have fabricated phase-transitional ionogel-based SCs for a selective operation. The electrolyte was made of ionogels using a phase-transitional IL as a solvent. Through a gelation, various disadvantages of liquid electrolytes, such as electrolyte leakage, corrosion, and packaging problems,[14] could be overcome. The ionogel was fabricated from acrylamide (AAm) monomers with a phase-transitional IL, 1-ethyl-3-methylimidazolium nitrate $[EMIM]^+[NO_3]^-$, as the ionogel solvent. The fabricated SC can be activated by elevating the temperature above the melting temperature, called an "operating mode". After operation, the SC can be converted into a "storage mode" by lowering the temperature, where self-discharge is reduced and there is no energy consumption to maintain energy storage. Since the ionogel electrolyte is stable even at a high temperature and can be selectively activated, we expect that SCs can be used in an environment with high temperatures or with large temperature variation such as a desert or a space industry.

MATERIALS AND METHODS

Fabrication of SCs. Carbon electrodes were prepared by coating aluminum foil with a mixture of activated carbon power (Sigma, C9157), Super P (Wellcos), and poly(vinylidene fluoride) (PVDF, Wellcos, #7300) in a ratio of 8:1:1. An ionogel solution was synthesized by mixing 12 wt % acrylamide (AAm, Sigma, A8887) to provide monomers for the polymer network, $[EMIM]^+[NO_3]^-$ (Iolitec, IL-0005-HP) as the ionogel solvent, 2.5 wt % poly(ethylene glycol) diacrylate (PEGDA; Sigma, 455008) as a crosslinker, and 0.4 wt % 2-hydroxy-4′-(2-hydroxyethoxy)-2-methylpropiophenone (Irgacure 2959, Sigma, 410896) as a photoinitiator. The ionogel solution was stirred for 1 h at 70 °C to create a homogeneous solution before polymerization. For preparation of the SCs, electrodes and a 1 mm-thick PDMS (Sylgard 184) mold were attached to Teflon tape to provide a flexible substrate. Then, the solution was poured into the PDMS mold and encapsulated with the same substrate. The solution

https://doi.org/10.1021/acsami.2c02160
ACS Appl. Mater. Interfaces 2022, 14, 23375−23382

was cured at a wavelength of 365 nm for 1 h to obtain phase-transitional ionogel-based SCs.

Ionogel Analysis. Ionogels were prepared in the same manner without the substrate. The transmittance of each ionogel sample was measured over a wavelength range of 300 to 400 nm using UV−vis spectroscopy (Agilent Technologies, Cary 60). Differential scanning calorimetry (DSC) was carried out using a TA Instruments Discovery DSC. The samples were analyzed at a heating rate of 2 °C min^{-1} over a temperature range of −20 to 100 °C. Mechanical tensile tests were performed to measure the mechanical property of the ionogel. A geometry of the sample with 30 mm in length, 10 mm in width, and 2 mm in thickness was used. The specimens were mounted to a tensile machine (Instron, 3343) and were stretched with a 50 N capacity load cell at a stretch rate of 10 mm s^{-1}. The initial length of the specimen between the grips was 5 mm. Fourier-transform infrared spectroscopy (FT-IR) (Thermo Scientific, Nicolet iS 10 spectrometer) was carried out to analyze the spectra of freeze-dried polyacrylamide, pure $[EMIM]^+[NO_3]^-$ IL, and the ionogel at 25 and 45 °C with wavenumbers from 550 to 4000 cm^{-1}. The cross section of an SC was characterized with a scanning electron microscope (SEM) (Carl Zeiss, AURIGA) at an accelerating voltage of 2 kV.

Characterization of Supercapacitor Electrochemical Properties. The performance of ionogel-containing SCs that were 18 mm in length, 8 mm in width, and 1 mm in thickness was evaluated using a two-electrode system. Electrochemical impedance spectroscopy (EIS), cyclic voltammetry (CV), and stability tests were carried out using a potentiostat/galvanostat (Gamry Reference 600+) with a two-electrode-system at various temperatures on a hot plate. The EIS test was performed in the frequency range of 0.1 Hz−1 MHz. The CV test was performed in the potential range of 0−2 V at various scan rates (12.5, 25, 50, 100, and 200 mV s^{-1}). The galvanostatic charge/discharge (GCD) curves were measured using a multichannel electrochemical workstation (ZIVE, MP1) at various current densities of 0.2, 0.5, 1, 2, and 4 A g^{-1} in a potential window of 0−2 V. The stability of SCs was measured by subjecting them to 3000 cyclic charge−discharge cycles in the potential range of 0−2 V at a current density of 0.5 A g^{-1} to measure capacitance retention.

Self-Discharging Test. The SC was charged to 1.85 V with a current density of 0.02 A g^{-1} and held at this terminal voltage for 2 h at 45 °C to ensure the fully charging. The open circuit voltage (OCV) was measured for 24 h in two cases of SCs at room temperature (25 °C) and 45 °C. To demonstrate usability of SCs, they were charged to 2 V for 2 h at 45 °C and solidified by lowering the temperature. After this, they were connected to LED lights (LUG30243/G-C, 155 Ω, ICbanQ). The photos of the LED light were recorded, and the light powers of the LED were measured using an optical power meter (Newport, 1919-R). LED experiments and measurements were conducted in a dark room.

RESULTS AND DISCUSSION

Phase-Transitional Characteristics of the Ionogel. The characteristics of the synthesized ionogel electrolyte for the phase-transitional SCs are illustrated in Figure 1a. Acrylamide monomers became polyacrylamide and formed a 3D matrix in the IL through chemical crosslinking with PEGDA when induced by the photoinitiator. Below the melting point, the IL ions are crystallized. Therefore, the movement of ions is suppressed. When the temperature is raised above the melting point of the IL, the IL ions are decrystallized, allowing the ions to move freely. To observe the crystallization−decrystallization change of IL according to the phase, X-ray diffraction (XRD) analysis was conducted (Figure S1). The data exhibit a clear difference in crystallinity at 25 and 45 °C. The structural formulas of the phase-transitional IL, $[EMIM]^+[NO_3]^-$, polyacrylamide (PAAm), and PEGDA constituting the ionogel electrolyte are shown in Figure 1b. All components are miscible with the IL to form a homogeneous solution. DSC measurements were carried out to investigate the phase transition temperature of pure $[EMIM]^+[NO_3]^-$ IL and $[EMIM]^+[NO_3]^-$/PAAm ionogels. (Figure 1c). The DSC results show that the melting point of the IL is 44.7 °C, while that of the ionogel is 44.8 °C. To precisely observe changes in transparency in the visible region, the transmittance of the 1 mm-thick ionogel was measured in the wavelength range of 400 to 800 nm using spectroscopy (Figure 1d). According to the transmittance spectra, the crystallized ionogel shows very low transmittance of less than 10%, while the decrystallized ionogel shows high transmittance of more than 90%. Below the melting point, a phase-transitional IL is known to form a crystal lattice.[10] Therefore, the difference in transmittance is the result of crystallized−decrystallized motion of the ionogel as the phase transition depending on the temperature. In order to compare the state of the ionogel at different temperatures, an ionogel sample with a size of 10 × 10 × 2 mm^3 was prepared (Figure 1e). At room temperature (25 °C), the ionogel was crystallized and appeared to be rigid and opaque, while the decrystallized ionogel at 45 °C appeared to be transparent and flexible. To analyze the chemical compositions of the ionogel, we have carried out FT-IR of polyacrylamide, pure $[EMIM]^+[NO_3]^-$, IL at 25 °C, and the ionogel at 25 and 45 °C (Figure 1f). In the spectrum of the ionogel, adsorption peaks located at 3387 and 1683 cm^{-1} were assigned to the N−H stretching and C═O stretching on polyacrylamide. The yellow and green regions (3140−3055 and 2971−2883 cm^{-1}) are assigned to the sp^2 C−H stretching and sp^3 C−H stretching, respectively. The peak located at 1332 cm^{-1} is attributed to the N═O stretching of nitrate ions. The bands located at 1575, 1635, and 1172 cm^{-1} are assigned to C═N stretching vibration, C═C stretching, and C−N stretching vibration of the imidazole ring, respectively.[15] The peak near 1172 cm^{-1} of polyacrylamide is attributed to the C−O stretch of the PEGDA crosslinker. It is confirmed that peaks of the ionogel at 25 °C are similar to those of IL at 25 °C, while the ionogel at 45 °C is similar to polyacrylamide in yellow and green regions. To investigate the mechanical properties of the ionogel, stress−strain tensile tests were carried out. Figure 1g shows the stress−strain curves of the ionogel according to temperature. The crystallized ionogel exhibits rigid physical properties by showing an elastic modulus value of 40.8 MPa and an elongation of 15%, whereas the decrystallized ionogel exhibits soft physical properties by showing an elastic modulus value of 26.9 kPa and an elongation of 272%. The tensile cyclic stress−strain curve of the ionogel up to a strain of 100% at 45 °C shows little physical deformation during 500 cycles, demonstrating high robustness (Figure 1h). Furthermore, by applying various sequential mechanical deformations to the ionogel, it was verified that the ionogel is sufficiently robust (Figure S2). Since polymers usually undergo rapid degradation, changes in electrochemical performance according to phase transition were considered.[16,17] During the phase transition, negligible volume change was observed (Figure S3). Moreover, the uniform distribution of IL ions did not change during repeated phase transitions (Figure S4). Therefore, the electrochemical performance degradation of the electrolyte during phase transition caused by the volume change and ion distribution change did not occur.

Selective Operation of SCs in Operating Mode and Storage Mode. We synthesized phase-transitional SCs based on the $[EMIM]^+[NO_3]^-$ ionogel electrolyte with carbon electrodes. The SC fabrication process is illustrated in Figure 2a. SCs were composed of Teflon tape as a flexible and

https://doi.org/10.1021/acsami.2c02160
ACS Appl. Mater. Interfaces 2022, 14, 23375−23382

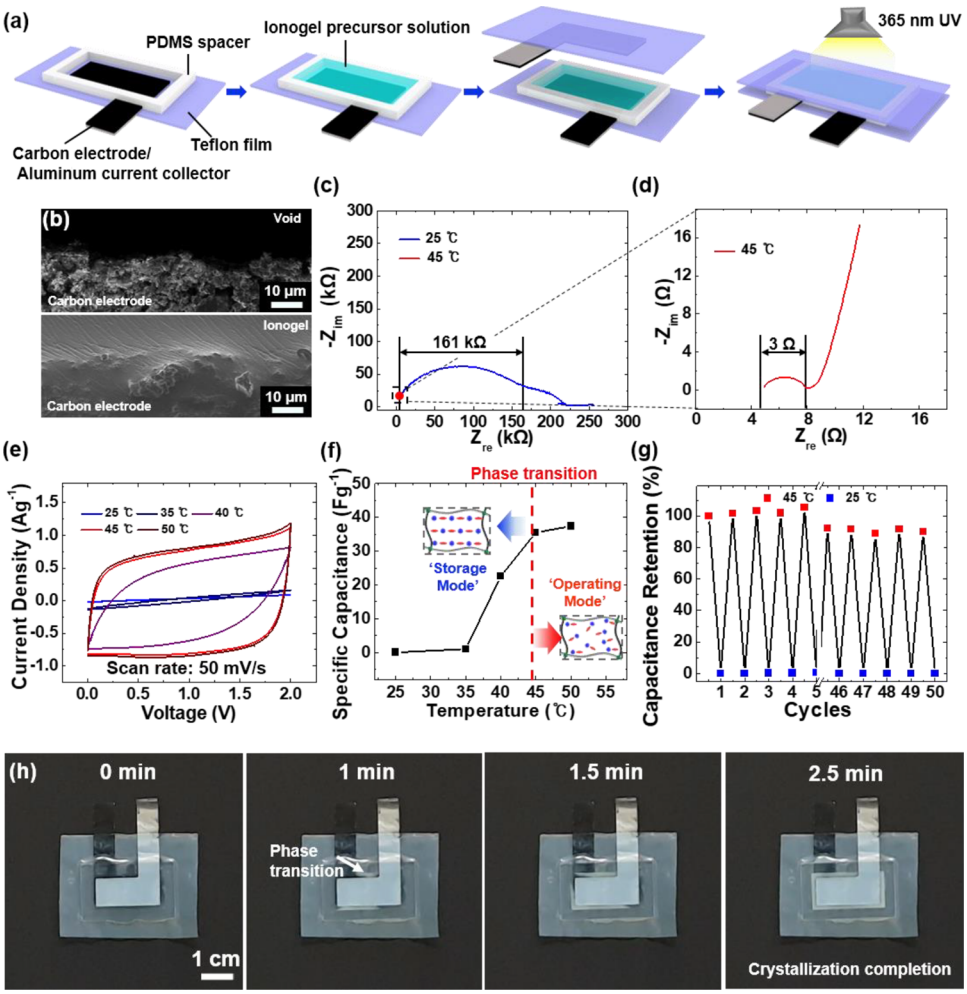

Figure 2. Phase-transitional supercapacitors (SCs). (a) Fabrication process of phase-transitional SCs. (b) SEM images of the ionogel/electrode interface of the SCs. A highly porous surface of the carbon electrode was observed. When the ionogel was polymerized on the carbon electrode, the interface of the ionogel and the electrode was robustly bonded. (c) Electrochemical impedance spectroscopy (EIS) curves of a storage mode of supercapacitor (SC_{SM}) and an operating mode of supercapacitor (SC_{OM}). Resistance of the SCs under ambient temperature of RT was 161 kΩ and (d) dramatically decreased up to 3 Ω with phase transition of the ionogel at 45 °C. (e) Cyclic voltammetry (CV) curves of SCs under ambient temperature from 25 to 50 °C. (f) Specific capacitance of a supercapacitor at different temperatures. The operating mode and storage mode were separated by the phase transition. (g) Reversibility of capacitance according to the temperature cycles; red dot: 45 °C; blue dot: 25 °C. (h) Real-time phase transition of the SC. After lowering the temperature from 45 to 25 °C, the phase transition started after 1 min and crystallization was completed after 2.5 min.

moisture proofing substrate, aluminum foil as a current collector, carbon electrodes, PDMS mold, and ionogel electrolyte. The PDMS mold served as a framework for fabrication of the bulky ionogel and prevented substrate separation when the SCs were bent. When manufacturing the ionogel electrolyte, in situ polymerization was performed to ensure perfect bonding between the electrode and the surface of the electrolyte[18] so that the bonding surface did not deviate during phase transition or bending. Figure 2b shows cross-sectional SEM images of the electrolyte/electrode surface. The image of the carbon electrode without the ionogel revealed a highly porous carbon surface. When the ionogel electrolyte was added, a strongly bonded surface of the ionogel and carbon electrode was observed. To observe the porous polymer network, the IL of the ionogel was replaced with deionized water for 3 days and freeze dried. Then, SEM images of the cross section of the dried ionogel were taken (Figure S5). We classified SCs into an operating mode of supercapacitor (SC_{OM}) and storage mode of supercapacitor (SC_{SM}) according to the phase of the ionogel electrolyte. Figure 2c,d shows the Nyquist plots for SC_{OM} and SC_{SM}. The plots reveal a semicircle at high frequencies, a nonvertical line at intermediate frequencies, and a sloping line at low frequencies. The diameter of the semicircle is assigned to the sum of the electrolyte resistance in the porous electrode and the electrode resistance.[19] The measured resistivity values were 2318.4 kΩ·cm and 43.2 Ω·cm for SC_{SM} and SC_{OM}, respectively, for a difference of about 53,600 times. Peculiarly, SC_{SM} showed a large nonvertical line following the semicircle with a value of 835.2 kΩ·cm. This tendency seems to be due to the large diffuse layer resistance in the solid phase.[20] Due to this dramatic difference in resistance, the activation−deactivation of the SCs is determined by temperature. The CV curve was derived to evaluate the performance of the phase-transitional SCs (Figure 2e,f). The SCs were measured at various temperatures (25 and 35, 40, 45, and 50 °C) at a scan rate of 50 mV s^{-1}. The CV curves show that SCs perform very poorly at 25 and 35 °C. They are activated as the temperature

https://doi.org/10.1021/acsami.2c02160
ACS Appl. Mater. Interfaces 2022, 14, 23375−23382

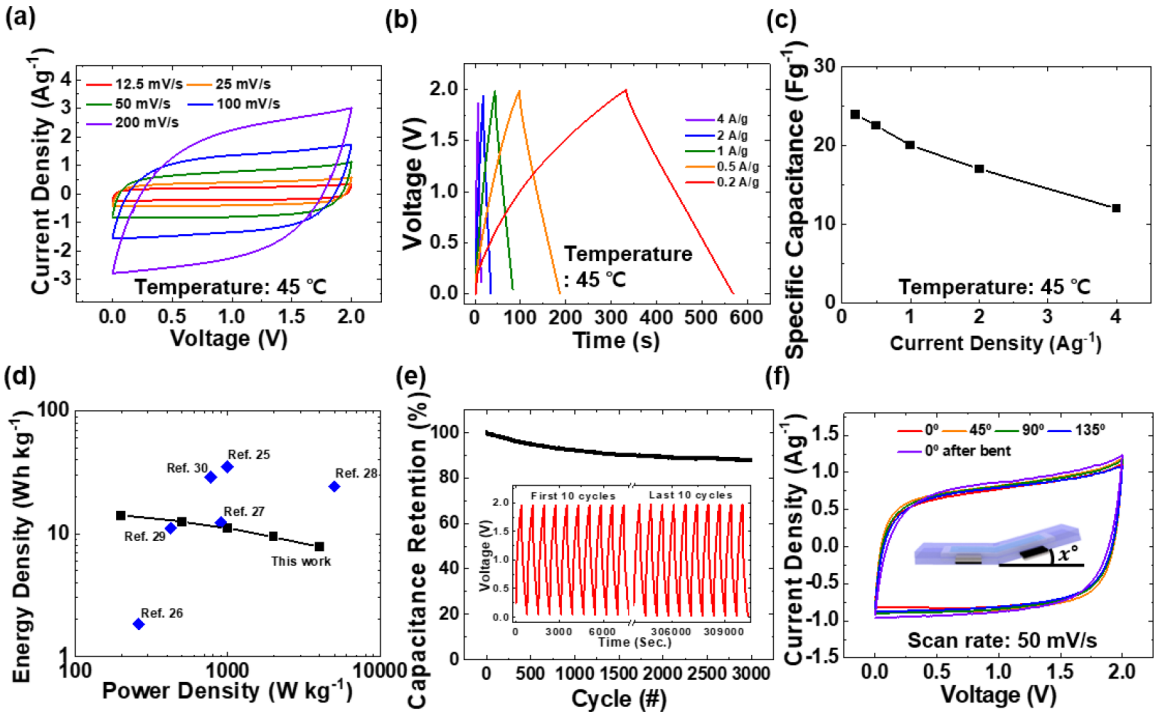

Figure 3. Electrochemical performance of phase-transitional SCs in operating mode. (a) Cyclic voltammetry curves of SC_{OM} at different scan rates from 12.5 to 200 mV s^{-1}. (b) Galvanostatic charge/discharge curves and (c) specific capacitance at current densities of 0.2, 0.5, 1, 2, and 4 A g^{-1}. (d) Ragone plot of the power density versus energy density for SC_{OM}. (e) Cyclic stability of SC_{OM} under an applied current density of 0.5 A g^{-1}. The inset shows charge−discharge cycles at the first 10 and final 10 stages. (f) Cyclic voltammetry curves of SC_{OM} under bending deformation. Softness of the SCs and the robust interface of electrode/ionogel yielded stable electrochemical performance.

approaches the melting point and become fully operational above the melting point of 41.3 °C. It is also shown that the SCs are very stable at a high temperature of 50 °C. These results are confirmed by the specific capacitance values at different temperatures. At 25 and 35 °C, specific capacitances are almost zero (0.02 and 1.04 F g^{-1}, respectively). As the temperature is gradually increased, the solid and liquid phases coexist at 40 °C, resulting in a specific capacitance of 22.57 F g^{-1}. Finally, the specific capacitance exceeds 37.35 F g^{-1} above the melting point. To compare the electrochemical performance of the pure IL electrolyte-based SC, a similar SC but with an $[EMIM]^+[NO_3]^-$ IL electrolyte was fabricated, and the electrochemical performance was measured (Figure S6). Since the ionogel is mostly composed of IL, IL-based SCs exhibit similar performance to ionogel-based SCs. To confirm that the activate/deactivate motion of the SCs is repeatable and evaluate the cycling life, the specific capacitances were measured by deriving the CV curve 50 cycles at 25 and 45 °C at a scan rate of 50 mV s^{-1}. Then, the capacitance retention was calculated based on the specific capacitance value at the first cycle at 45 °C, as shown in Figure 2g. Active/inactive motions are clearly observed during several cycles, and capacitance retention was decreased about 10% after 45 cycles. Figure 2h shows the real-time phase transition of the SC. The temperature of SC_{OM} at 45 °C was lowered to 25 °C. In the ionogel electrolyte of the SC, the phase transition began after 1 min and crystallization was fully completed after 2.5 min.

Capacitive Performance of SCs in Operating Mode. To measure the capacitive performance of SC, SC_{OM} was evaluated at 45 °C. At this point, the SC was fully operational in the two-electrode configuration. Figure 3a shows the CV measurements between 0 and 2 V at various scan rates from 5 to 200 mV s^{-1}. The rectangular shape of the CV curves at all scan rates indicates good capacitive behavior.[21] At a high scan rate of 200 mV s^{-1}, the rectangular shape of the CV curve is slightly distorted because there is insufficient time for interactions between the electrode and electrolye.[22] The capacitive performance at different current densities was further confirmed by the GCD curves (Figure 3b). All GCD curves maintain a nearly symmetrical triangular shape at different current densities (0.2, 0.5, 1, 2, and 4 A g^{-1}) in the potential window of 0−2 V, indicating a high degree of reversibility in the charge/discharge process.[23] Based on the GCD measurements, the specific capacitance was calculated according to the current density (Figure 3c). When the current density was 0.2 A g^{-1}, the capacitance was 25.2 F g^{-1}, and the capacitance gradually decreased as the current density increased. Figure 3d reveals the relationship between the energy density and power density of the SCs (Ragone plot). The SC_{OM} exhibited an energy density of 7.77 Wh kg^{-1} at a power density of 4000 W kg^{-1}. The energy density and power density in this work are comparable to the performance of the previously reported carbon electrode and IL such as $[Emim]^+[OAc]^-$,[24] $[C_4mim]^+[OAc]^-$,[25] $[Emim]^+[Cl]^-$,[26] $[EMIH]^+[SO_4]^-$,[27] $[Pyr_{14}]^+[Br]^-$,[28] and $[EMIM]^+[BF_4]^-$[29] based SCs (Figure 3d). The long-term cyclic stability of SC_{OM} was also examined using a cyclic charge−discharge system at a current density of 0.5 A s^{-1}, as shown in Figure 3e. The capacitance retention reached 87.5% after 3000 cycles, suggesting good electrochemical stability. Figure 3f shows the curves of SC_{OM} at different folding angles (pristine, 45°, 90°, 135°, and 0°). The shapes of the CV curve show a negligible amount of change under all folding angles, indicating that the capacitive property of the SCs is not significantly affected by

https://doi.org/10.1021/acsami.2c02160
ACS Appl. Mater. Interfaces 2022, 14, 23375−23382

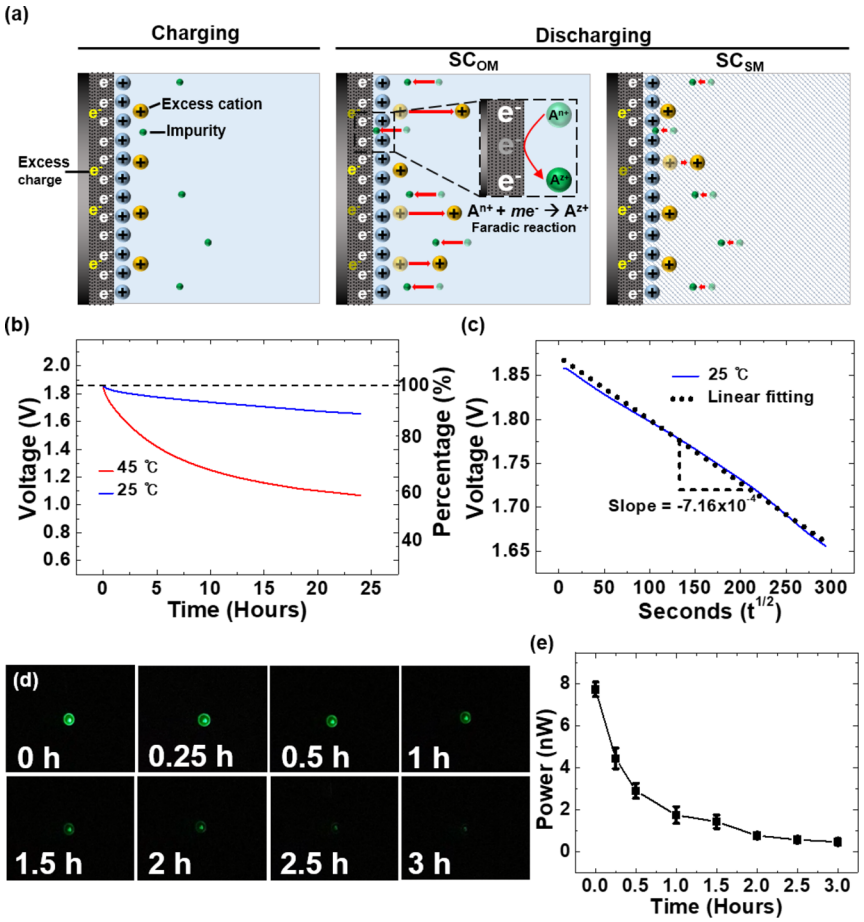

Figure 4. Suppressed self-discharges of phase-transitional SCs in storage mode. (a) Schematic illustrations of charging and self-discharging processes of SC_{SM} and SC_{OM}. Self-discharge was described with a diffusion-controlled model. (b) Self-discharging curves of an SC at 45 and 25 °C. (c) Self-discharging curve of a supercapacitor at 25 °C. The curve is fitted by the diffusion-controlled model. The measured diffusion parameter m is 7.16×10^{-4} V $s^{-1/2}$. (d,e) Suppressed self-discharging of the SC enhances optical power duration of a green LED during a discharging process.

folding stress.[30] This is due to the flexibility of the ionogel. In addition, since the electrode and electrolyte are combined into one entity through in situ polymerization, there is no deviation even when folded.

Self-Discharge Characteristics of SCs in Storage Mode. We have explored SC_{SM} that can suppress the movement of ions to reduce the self-discharge, which is a main drawback of SCs.[31] There are three mechanisms that describe the self-discharge: ohmic leakage, diffusion-controlled faradaic process, and activation-controlled faradaic process.[32,33] Among them, the diffusion-controlled faradaic process acted as the main self-discharge factor in our SCs. The diffusion-controlled model is expressed by eq 1, where m is the diffusion parameter, the diffusion rate of the ions near the electrode surface.[34]

$$V = V_o - m\sqrt{t} \quad (1)$$

The diffusion-controlled process is caused by the following mechanism. (1) Impurities such as Fe^{2+}/Fe^{3+} or O_2 create a shuttle effect.[35] Then, faradaic reaction occurs by diffusion of depolarizing impurities into the electrode, causing charge leakage.[36] (2) During charging, the local ionic concentration at or near the carbon increases. After disconnection, some excess ions diffuse to an equilibrium state, reducing the charge in the carbon.[33] At room temperature, the ionogel electrolyte crystallizes to inhibit the diffusion of impurities and excess ions. Therefore, the self-discharge of SC_{SM} can be sufficiently suppressed. Figure 4a shows a schematic illustration of ion diffusion in SC_{OM} and SC_{SM}. After discharging, since excess ions and impurities can move easily in SC_{OM}, diffusion occurs. Therefore, charges are reduced by faradic reaction by cation impurities at the electrode and diffusion of excess ions. On the other hand, ions are crystallized and much less diffusion occurs in SC_{SM}. Therefore, after charging at a high temperature, an SC is capable of storing charge for a long time in room temperature. To verify the effect of phase transition on self-discharge, the SCs were charged to 1.85 V with a current density of 0.02 A g^{-1} and held at this terminal voltage for 2 h at 45 °C. Under the same conditions, the GCD curve was derived and it was found that the energy density value is 22.71 Wh kg^{-1} (Figure S7). Then, self-discharge was measured in two cases, SC_{SM} at room temperature and SC_{OM} at 45 °C, through OCV for 24 h (Figure 4b). In order to minimize the activation-controlled faradaic process, self-discharge caused by over-charging,[37] the voltage was set to 1.85 V based on the stability window shown in the CV curve. According to the OCV curves, 57.79% of the initial voltage was maintained at 45 °C after 24 h, while 89.51% was maintained at room temperature. This observation points to the outstanding performance over the existing IL-based SCs (Table 1). Figure 4c shows a fitted graph to which the diffusion-controlled model is applied. The self-discharge curve has a linear relationship between V and $t^{1/2}$,

https://doi.org/10.1021/acsami.2c02160
ACS Appl. Mater. Interfaces 2022, 14, 23375−23382

Table 1. Self-Discharge Performance of Ionic Liquid-Based SCs

ionic liquid	charging voltage [V]	discharging time [h]	self-discharge rate [%]	ref
$[EMIM]^+[Ac]^-$	1.5	3	20	38
$[BMIM]^+[Br]^-$	1.8	5	34.4	39
$[TEMA]^+[BF_4]^-$	2	24	29	7
$[EMIM]^+[BF_4]^-$	3	60	28.9	34
$[EMIM]^+[NO_3]^-$	1.85	24	10.49	this work

and the correlation coefficient R^2 is more than 0.99. Furthermore, the diffusion parameter m is 7.16×10^{-4} V $s^{-1/2}$, much lower than that of the conventional SCs (3×10^{-3}~19×10^{-3} V $s^{-1/2}$).[33] This result indicates that the crystallized ionogel electrolyte effectively inhibits the movement of ions and impurities. As a result, self-discharge by diffusion was effectively suppressed. We represent the effect of ohmic leakage through a fitted graph (Figure S8). Given that the graph is poor fit, it is concluded that ohmic leakage is also not a major factor. In order to demonstrate the practical usability of the synthesized SCs, they were connected to LED lights (Figure S9). Each SC was charged to 2 V for 2 h at 45 °C and then crystallized by lowering the temperature to room temperature. Photographs of the green LED at each time point are presented in Figure 4d, and the DC light power of green LED output over time is plotted in Figure 4e. The LED light remained on for more than 3 h. Since self-discharge was minimized by controlling the ionic conductivity of the SCs, most of the charging voltage could be used to turn on the LED.

CONCLUSIONS

In this study, we presented an SC based on a phase-transitional ionogel electrolyte for a selective operating/storage mode. To overcome various disadvantages of IL electrolytes, such as leakage, corrosion, and packaging problems, a phase-transitional IL and a polymer were combined using a photoinitiator to fabricate the ionogel electrolyte. In the ionogel manufacturing process, the bonding strength between the electrode and the electrolyte was improved through in situ polymerization. By controlling the phase with a change in temperature, the ionogel can be made to be rigid and opaque below the melting point, whereas it is flexible and transparent above the melting point. The EIS data show a dramatic difference in resistance depending on the phase, indicating the effective control of ionic conduction. We investigated how the performance of the SCs changes with temperature. The results of the CV test confirmed that the phase-transitional SCs are activated/deactivated and show significant differences in capacitance with changes in temperature. To evaluate the capacitive performance of the SCs, CV and GCD tests were performed above the melting point in the operating mode. The SC_{OM} showed good capacitive behavior, high reversibility, stability, and flexibility. In the storage mode, it was shown that self-discharge was significantly suppressed through a diffusion-controlled model. Therefore, it was confirmed that the LED device was turned on for a long time. We expect that phase-transitional SCs provide a better development and understanding of an energy storage device in the future.

ASSOCIATED CONTENT

Supporting Information

The Supporting Information is available free of charge at https://pubs.acs.org/doi/10.1021/acsami.2c02160.

Electrochemical performance evaluation equation; XRD, DSC, and SEM; photos of various sequential mechanical deformations, volume change, ion distribution, and LED operation; electrochemical performance measurement of the ionic liquid supercapacitor, GCD curves, and the self-discharge curve (PDF)

AUTHOR INFORMATION

Corresponding Author

Jeong-Yun Sun − *Department of Material Science and Engineering and Research Institute of Advanced Materials (RIAM), Seoul National University, Seoul 08826, South Korea;* orcid.org/0000-0002-7276-1947; Email: jysun@snu.ac.kr

Author

Jinwoo Park − *Department of Material Science and Engineering, Seoul National University, Seoul 08826, South Korea*

Complete contact information is available at: https://pubs.acs.org/doi/10.1021/acsami.2c02160

Author Contributions

J.P. conceived the idea, designed the experiments, contributed to materials fabrication and characterization, evaluated electrochemical performance, and wrote the main manuscript. J.-Y.S. supervised the study and provided intellectual and technical guidance. All authors discussed the results and commented on the manuscript.

Notes

The authors declare no competing financial interest.

ACKNOWLEDGMENTS

This work was supported by National Research Foundation of Korea (NRF) grants funded by the Korean government (no. 2017M3D9A1073922, 2018M3A7B4089670, and 2021R1A2C2092737).

REFERENCES

(1) Frackowiak, E.; Béguin, F. *Supercapacitors: Materials, Systems and Applications*; Wiley-VCH Verlag GmbH & Co: Poznan, 2013; pp 289−305.

(2) González, A.; Goikolea, E.; Barrena, J. A.; Mysyk, R. Review on Supercapacitors: Technologies and Materials. *Renewable Sustainable Energy Rev.* **2016**, *58*, 1189−1206.

(3) Banerjee, S.; De, B.; Sinha, P.; Cherusseri, J.; Kar, K. K. Applications of Supercapacitors. In *Handbook of Nanocomposite Supercapacitor Materials I*; Springer, 2020; pp 341−350.

(4) Kowal, J.; Avaroglu, E.; Chamekh, F.; Šenfelds, A.; Thien, T.; Wijaya, D.; Sauer, D. U. Detailed Analysis of the Self-Discharge of Supercapacitors. *J. Power Sources* **2011**, *196*, 573−579.

(5) Zhang, W.; Yang, W.; Zhou, H.; Zhang, Z.; Zhao, M.; Liu, Q.; Yang, J.; Lu, X. Self-discharge of Supercapacitors Nased on Carbon Nanotubes with Different Diameters. *Electrochim. Acta* **2020**, *357*, No. 136855.

(6) Wang, H.; Zhou, Q.; Yao, B.; Ma, H.; Zhang, M.; Li, C.; Shi, G. Suppressing the Self-Discharge of Supercapacitors by Modifying Separators with an Ionic Polyelectrolyte. *Adv. Mater. Interfaces* **2018**, *5*, No. 1701547.

(7) Xia, M.; Nie, J.; Zhang, Z.; Lu, X.; Wang, Z. L. Suppressing Self-Discharge of Supercapacitors Via Electrorheological Effect of Liquid Crystals. *Nano Energy* **2018**, *47*, 43−50.
(8) Liu, M.; Xia, M.; Qi, R.; Ma, Q.; Zhao, M.; Zhang, Z.; Lu, X. Lyotropic Liquid Crystal as an Electrolyte Additive for Suppressing Self-Discharge of Supercapacitors. *ChemElectroChem* **2019**, *6*, 2531−2535.
(9) Lei, Z.; Chen, B.; Koo, Y.-M.; MacFarlane, D. R. Introduction: Ionic Liquids. *Chem. Rev.* **2017**, *117*, 6633−6635.
(10) Ming, X.; Shi, L.; Zhu, H.; Zhang, Q. Stretchable, Phase-Transformable Ionogels with Reversible Ionic Conductor−Insulator Transition. *Adv. Funct. Mater.* **2020**, *30*, No. 2005079.
(11) Feng, J.; Wang, Y.; Xu, Y.; Sun, Y.; Tang, Y.; Yan, X. Ion Regulation of Ionic Liquid Electrolytes for Supercapacitors. *Energy Environ. Sci.* **2021**, *14*, 2859−2882.
(12) Dou, Q.; Liu, L.; Yang, B.; Lang, J.; Yan, X. Silica-Grafted Ionic Liquids for Revealing the Respective Charging Behaviors of Cations and Anions in Supercapacitors. *Nat. Commun.* **2017**, *8*, 2188.
(13) Feng, J.; Wang, Y.; Xu, Y.; Ma, H.; Wang, G.; Ma, P.; Tang, Y.; Yan, X. Construction of Supercapacitor-Based Ionic Diodes with Adjustable Bias Directions by Using Poly (ionic liquid) Electrolytes. *Adv. Mater.* **2021**, *33*, No. 2100887.
(14) Karuppasamy, K.; Theerthagiri, J.; Vikraman, D.; Yim, C.-J.; Hussain, S.; Sharma, R.; Maiyalagan, T.; Qin, J.; Kim, H.-S. Ionic Liquid-Based Electrolytes for Energy Storage Devices: a Brief Review on Their Limits and Applications. *Polymer* **2020**, *12*, 918.
(15) Ndruru, S. T. C. L.; Widiarto, S.; Pramono, E.; Wahyuningrum, D.; Bundjali, B.; Arcana, I. M. The Influences of [EMIm] Ac Ionic Liquid for The Characteristics of Li-ion Batteries Solid Biopolymer Blend Electrolyte Based on Cellulose Derivatives of MC/CMC Blend. *Macromol. Chem. Phys.* **2022**, *223*, No. 2100362.
(16) Chu, X.; Zhao, X.; Zhou, Y.; Wang, Y.; Han, X.; Zhou, Y.; Ma, J.; Wang, Z.; Huang, H.; Xu, Z. An Ultrathin Robust Polymer Membrane for Wearable Solid-State Electrochemical Energy Storage. *Nano Energy* **2020**, *76*, No. 105179.
(17) Wang, Y.; Chu, X.; Zhu, Z.; Xiong, D.; Zhang, H.; Yang, W. Dynamically evolving 2D Supramolecular Polyaniline Nanosheets for Long-Stability Flexible Supercapacitors. *Chem. Eng. J.* **2021**, *423*, No. 130203.
(18) Anothumakkool, B.; Torris, A. T. A.; Veeliyath, S.; Vijayakumar, V.; Badiger, M. V.; Kurungot, S. High-Performance Flexible Solid-State Supercapacitor with an Extended Nanoregime Interface Through in Situ Polymer Electrolyte Generation. *ACS Appl. Mater. Interfaces* **2016**, *8*, 1233−1241.
(19) Lei, C.; Markoulidis, F.; Ashitaka, Z.; Lekakou, C. Reduction of Porous Carbon/Al Contact Resistance for an Electric Double-Layer Capacitor (EDLC). *Electrochim. Acta* **2013**, *92*, 183−187.
(20) Mei, B.-A.; Munteshari, O.; Lau, J.; Dunn, B.; Pilon, L. Physical Interpretations of Nyquist Plots for EDLC Electrodes and Devices. *J. Phys. Chem. C* **2018**, *122*, 194−206.
(21) Xue, Q.; Gan, H.; Huang, Y.; Zhu, M.; Pei, Z.; Li, H.; Deng, S.; Liu, F.; Zhi, C. Boron Element Nanowires Electrode for Supercapacitors. *Adv. Energy Mater.* **2018**, *8*, No. 1703117.
(22) Mujawar, S. H.; Ambade, S. B.; Battumur, T.; Ambade, R. B.; Lee, S.-H. Electropolymerization of Polyaniline on Titanium Oxide Nanotubes for Supercapacitor Application. *Electrochim. Acta* **2011**, *56*, 4462−4466.
(23) Gao, M.; Wu, X.; Qiu, H.; Zhang, Q.; Huang, K.; Feng, S.; Yang, Y.; Wang, T.; Zhao, B.; Liu, Z. Reduced Graphene Oxide-Mediated Synthesis of Mn_3O_4 Nanomaterials for an Asymmetric Supercapacitor Cell. *RSC Adv.* **2018**, *8*, 20661−20668.
(24) Guo, S.; Zhao, K.; Feng, Z.; Hou, Y.; Li, H.; Zhao, J.; Tian, Y.; Song, H. High Performance Liquid Crystalline Bionanocomposite Ionogels Prepared by in Situ Crosslinking of Cellulose/Halloysite Nanotubes/Ionic Liquid Dispersions and Its Application in Supercapacitors. *Appl. Surf. Sci.* **2018**, *455*, 599−607.
(25) Trivedi, T. J.; Bhattacharjya, D.; Yu, J. S.; Kumar, A. Functionalized Agarose Self-Healing Ionogels Suitable for Supercapacitors. *ChemSusChem* **2015**, *8*, 3294−3303.
(26) Wu, J.; Xia, G.; Li, S.; Wang, L.; Ma, J. A Flexible and Self-Healable Gelled Polymer Electrolyte Based on a Dynamically Cross-Linked PVA Ionogel for High-Performance Supercapacitors. *Ind. Eng. Chem. Res.* **2020**, *59*, 22509−22519.
(27) Yadav, N.; Yadav, N.; Hashmi, S. Ionic Liquid Incorporated, Redox-Active Blend Polymer Electrolyte for High Energy Density Quasi-Solid-State Carbon Supercapacitor. *J. Power Sources* **2020**, *451*, No. 227771.
(28) Geng, C.-L.; Fan, L.-Q.; Wang, C.-Y.; Wang, Y.-L.; Sun, S.-J.; Song, Z.-Y.; Liu, N.; Wu, J.-H. High Energy Density and High Working Voltage of a Quasi-Solid-State Supercapacitor with a Redox-Active Ionic Liquid Added Gel Polymer Electrolyte. *New J. Chem.* **2019**, *43*, 18935−18942.
(29) Karnan, M.; Raj, A. K.; Subramani, K.; Santhoshkumar, S.; Sathish, M. The Fascinating Supercapacitive Performance of Activated Carbon Electrodes with Enhanced Energy Density in Multifarious Electrolytes. *Sustainable Energy Fuels* **2020**, *4*, 3029−3041.
(30) Xie, Y.; Liu, Y.; Zhao, Y.; Tsang, Y. H.; Lau, S. P.; Huang, H.; Chai, Y. Stretchable All-Solid-State Supercapacitor with Wavy Shaped Polyaniline/Graphene Electrode. *J. Mater. Chem. A* **2014**, *2*, 9142−9149.
(31) Tevi, T.; Takshi, A. Modeling and Simulation Study of the Self-Discharge in Supercapacitors in Presence of a Blocking Layer. *J. Power Sources* **2015**, *273*, 857−862.
(32) Conway, B. E.; Pell, W.; Liu, T. Diagnostic Analyses for Mechanisms of Self-Discharge of Electrochemical Capacitors and Batteries. *J. Power Sources* **1997**, *65*, 53−59.
(33) Ricketts, B.; Ton-That, C. Self-Discharge of Carbon-Based Supercapacitors with Organic Electrolytes. *J. Power Sources* **2000**, *89*, 64−69.
(34) Wang, Z.; Chu, X.; Xu, Z.; Su, H.; Yan, C.; Liu, F.; Gu, B.; Huang, H.; Xiong, D.; Zhang, H. Extremely Low Self-Discharge Solid-State Supercapacitors Via the Confinement Effect of Ion Transfer. *J. Mater. Chem. A* **2019**, *7*, 8633−8640.
(35) Wang, Z.; Xu, Z.; Huang, H.; Chu, X.; Xie, Y.; Xiong, D.; Yan, C.; Zhao, H.; Zhang, H.; Yang, W. Unraveling and Regulating Self-Discharge Behavior of $Ti_3C_2T_x$ MXene-Based Supercapacitors. *ACS Nano* **2020**, *14*, 4916−4924.
(36) Hess, L.; Fulik, N.; Röhner, J.; Zhang, E.; Kaskel, S.; Brunner, E.; Balducci, A. The Role of Diffusion Processes in the Self-Discharge of Electrochemical Capacitors. *Energy Storage Mater.* **2021**, *37*, 501−508.
(37) Lewandowski, A.; Jakobczyk, P.; Galinski, M.; Biegun, M. Self-Discharge of Electrochemical Double Layer Capacitors. *Phys. Chem. Chem. Phys.* **2013**, *15*, 8692−8699.
(38) Haque, M.; Li, Q.; Rigato, C.; Rajaras, A.; Smith, A. D.; Lundgren, P.; Enoksson, P. Identification of Self-Discharge Mechanisms of Ionic Liquid Electrolyte Based Supercapacitor Under High-Temperature Operation. *J. Power Sources* **2021**, *485*, No. 229328.
(39) Fan, L.-Q.; Tu, Q.-M.; Geng, C.-L.; Huang, J.-L.; Gu, Y.; Lin, J.-M.; Huang, Y.-F.; Wu, J.-H. High Energy Density and Low Self-Discharge of a Quasi-Solid-State Supercapacitor with Carbon Nanotubes Incorporated Redox-Active Ionic Liquid-Based Gel Polymer Electrolyte. *Electrochim. Acta* **2020**, *331*, No. 135425.

https://doi.org/10.1021/acsami.2c02160
ACS Appl. Mater. Interfaces 2022, 14, 23375−23382